

Original Article

A pilot study comparing the genetic molecular biology of gestational and non-gestational choriocarcinoma

Cordelle Lazare^{1*}, Wenhua Zhi^{1*}, Jun Dai¹, Canhui Cao¹, Rajiv Rai Sookha¹, Ling Wang¹, Yifan Meng¹, Peipei Gao¹, Ping Wu¹, Juncheng Wei^{1,2}, Junbo Hu¹, Peng Wu^{1,2}

¹The Key Laboratory of Cancer Invasion and Metastasis of The Ministry of Education of China, Tongji Hospital, Tongji Medical College, Huazhong University of Science and Technology, Wuhan, Hubei Province, China;

²Department of Gynecologic Oncology, Tongji Hospital, Tongji Medical College, Huazhong University of Science and Technology, Wuhan, Hubei Province, China. *Equal contributors and co-first authors.

Received July 18, 2019; Accepted October 30, 2019; Epub November 15, 2019; Published November 30, 2019

Abstract: Non-gestational choriocarcinoma (NGC) is a rare subtype of choriocarcinoma differing in origin and phenotypic characteristics compared to gestational choriocarcinoma (GC). This study aimed to analyze the molecular biology of GC and NGC and evaluate genetic anomalies of choriocarcinoma subtypes. DNA was extracted and paired from tumor-normal tissue of one NGC and one GC (control) patient for whole-exome sequencing. To further understand the role of *DNAJB9*, a *p53* regulator mutated in the NGC tumor, on *p53* upregulation in choriocarcinoma, CRISPR/Cas9 was used to induce *DNAJB9* site-specific mutations in choriocarcinoma cells JEG-3. We hypothesized that *DNAJB9* dysfunction would result in *p53* overexpression. Sequencing revealed the GC tumor contained > 7 times more somatic mutations than the NGC tumor. Missense (98.86% vs. 94.97%), stop-gain (0.57% vs. 0.93%), and frameshift mutations (0.57% vs. 4.10%) were observed in the GC and NGC samples, respectively ($\chi^2 = 24.63$, $P < 0.00001$). The transition substitution rate was 67.54% and 55.71% in the GC and NGC samples, while the transversion substitution rate was 32.46% and 44.29% in the GC and NGC samples, respectively ($\chi^2 = 11.56$, $P < 0.000673$). Pathway enrichment analysis revealed ECM-receptor interaction and graft-versus-host disease were most enriched in the GC and NGC tumors, respectively. *In vitro* investigations showed that *DNAJB9* mRNA and protein levels were downregulated in Cas9-*DNAJB9*-sgRNA transfected cells compared to the control ($P < 0.001$), while *p53* protein levels were upregulated. Our findings display the genetic distinctness of choriocarcinoma subtypes, especially NGC, and further highlight the relationship between *p53* and *DNAJB9* in choriocarcinoma cells, laying the foundation for further investigations.

Keywords: Choriocarcinoma, *DNAJB9*, *p53*, whole exome sequencing, CRISPR/Cas9

Introduction

Choriocarcinoma is a highly aggressive, malignant trophoblastic neoplasm, which is vastly curable, and typically observed in women of childbearing age [1]. This tumor displays biphasic proliferation of the two cell types making up its composition, cytotrophoblasts, and syncytiotrophoblasts, with the latter being differentiated, non-dividing, and the hormone-secreting element of the tumor [2-4]. Choriocarcinoma is subcategorized into gestational choriocarcinoma (GC) and non-gestational choriocarcinoma (NGC). GC accounts for the majority of choriocarcinoma cases, usually occurring subsequent to a molar pregnancy or infrequently follow a non-molar pregnancy, and is genetically char-

acterized based on the presence or lack of a paternal chromosomal complement [5, 6]. The incidence rate of GC varies regionally, occurring in 1 in 20,000 to 40,000 pregnancies in western countries and 1 in 500 to 3,000 pregnancies in south-east Asia [7]. Unlike GC, NGC is not linked to any form of pregnancy and is the rarer subtype. This subtype originates from trophoblastic differentiation of germ cell tumors in the gonads or as a somatic component of another histologically different tumor such as teratoma, yolk sac tumor, embryonic carcinoma, and endometrioid adenocarcinoma; hence NGC only contains the patient's genetic material [8-10]. Even less commonly observed is intrauterine NGC [11]. The occurrence of either choriocarcinoma subtype in postmenopausal

Genetic similarities however with vast differences

Table 1. Patient demographics

	Patient 1	Patient 2
Age	23	50
Gender	Female	Female
Menstrual status	Premenopausal	Postmenopausal
Parity	G1P1	G3P3
Interval years from index pregnancy	< 1	25
Diagnosis	GC (I:6)	NGC (III:7)
Primary site	Intrauterine	Extrauterine
Metastasis	-	-
Chemotherapy	EMA-CO	EMA-CO
Surgical treatment	Total laparoscopic hysterectomy	Total transabdominal hysterectomy + bilateral adnexectomy + cytoreduction
Pathology	GC	NGC

Abbreviations: EMA-CO: etoposide, methotrexate, dactinomycin (actinomycin D), cyclophosphamide, vincristine (Oncovin); G1P1: gravida 1 para 1; G3P3: gravida 3 para 3; GC: gestational choriocarcinoma; NGC: non-gestational choriocarcinoma.

women is extremely rare, and when encountered sparks an immediate interest in the medical community [12].

Although the phenotypic differences between these choriocarcinoma subtypes are well defined, much less is known regarding their genotypic variances [1, 6, 9]. Several studies have employed the use of microsatellite genotyping and polymorphism for differentiation between GC and NGC, GC origin determination, and pinpoint identification of the causative pregnancy in GC [10, 13-16]. Nevertheless, there has been no prior use of next-generation sequencing (NGS), more specifically whole-exome sequencing (WES), to evaluate the molecular biology of either GC or NGC.

In this study, we aimed to analyze the genetic variation profiles of GC and NGC, explicitly highlighting the shared genetic events and signaling pathway associated somatically mutated genes, and further analyze the effect of stand-out mutations via *in vitro* investigation.

Materials and methods

Patient selection and tissue sample collection

Two patients were identified for this study: (1) a 23-year-old female diagnosed with GC and treated with a laparoscopic hysterectomy after one cycle of neoadjuvant chemotherapy (EMA-CO); (2) a 50-year-old female (25 years following antecedent pregnancy and two years postmenopausal) diagnosed with NGC involving the left round and broad ligaments, and the left fallopian tube, surgically treated with three cycles of neoadjuvant chemotherapy (EMA-CO)

followed by total transabdominal hysterectomy, bilateral adnexectomy, and cytoreduction (**Table 1**). Clinical staging and prognostic score were defined according to the International Federation of Gynecology and Obstetrics (FIGO) system and the prognostic scoring system of the WHO, respectively.

Archival formalin-fixed and paraffin-embedded (FFPE) tumor and adjacent non-tumor tissue samples of both patients were collected from the Department of Pathology, Tongji Hospital, Tongji Medical College, Huazhong University of Science and Technology. Histopathological diagnosis was based on the World Health Organization (WHO) classifications and executed by expert pathologists. This study was approved by the Ethics Committee of Tongji Medical College of Huazhong University of Science and Technology (TJ-IRB20180612). Informed and written consent was obtained from all subjects prior to the study.

DNA extraction and exome sequencing

Genomic DNA (gDNA) was extracted from 30 mg of the GC and NGC tumor and adjacent non-tumor tissue samples, using the QIAmp DNA FFPE Tissue Kit (Qiagen, Germany Cat# 56404) and the RNase A Kit (Qiagen, Germany Cat# 19101) according to the manufacturer's instructions. The DNA quality was evaluated using Qubit 3 Fluorometer (Invitrogen, USA) and agarose gel electrophoresis. The sequencing library was prepared using Aligent SureSelect All Human Exome Library (60 Mb) V6 (Agilent, USA). gDNA from each specimen was randomly sonicated to 140-200 bp and purified using magnetic beads. Fragments were then hybrid-

Genetic similarities however with vast differences

ized to the capture library. Dynal beads were subsequently used to capture the hybridized DNA fragments. The captured libraries were amplified using polymerase chain reaction (PCR) and then purified. The quality and quantity of the final library were analyzed by Qubit 3 Fluorometer and Aligent 2100 Bioanalyzer. Finally, sequencing was performed on the HiSeq X Ten (Illumina, USA).

Data analysis

The short reads were initially aligned using the Burrows Wheeler Aligner (BWA). Freebayes was used to recalibrate and filter alignments, and to highlight somatic mutations by comparing tumor against adjacent non-tumor tissue.

Somatic mutations were annotated by Annovar [17]. SIFT, PolyPhen2 HDIV, PolyPhen2 HVAR, and the Cosmic, Clinvar, and 1,000 Genome databases were used to predict the functional impacts of missense mutations. Variants were deemed deleterious mutations if at least two algorithms/databases scored them as deleterious. Any missense mutations which were recorded as unavailable by the algorithms/databases mentioned above were excluded from the analysis. Frameshift variants were categorized as pathogenic. All classifications used followed the standards and guidelines of the American College of Medical Genetics [18]. Circos was implemented for the visualization of overall genomic events in both tumor samples, while Maftools, an open-source R package, was implemented in lollipop plot and signature analysis visualization as previously described by Mayakonda et al. [19, 20]. All somatically mutated genes observed in this study were loaded into the Database for Annotation, Visualization, and Integrated Discovery (DAVID) v6.8 and the Kyoto Encyclopedia of Genes and Genomes (KEGG) database for pathway analysis [21-24]. Only pathways with P values ≤ 0.05 were included. Cytoscape was used for the visualization of these pathways [25].

Cell line and cell culture

The choriocarcinoma cell line, JEG-3, was used in this study (ATCC Cat# HTB-36). Cells were cultured in Dulbecco's modified Eagle's medium (DMEM) complemented with 10% fetal bovine serum (FBS), 100 $\mu\text{g}/\text{mL}$ streptomycin, and 100 units/mL of penicillin, and were cultivated at 37°C in a humidified atmosphere containing 5% CO_2 .

Immunohistochemistry

FFPE tumor tissue sections were subjected to deparaffinization and dehydration. Following H_2O_2 treatments and non-specific antigen blocking, slides were incubated with the following primary antibodies: DNAJB9 (1:50, GeneTex, USA Cat# GTX26053) and P53 (1:400, Proteintech, China Cat# 21891-1-AP) at 4°C. Subsequent to overnight incubation, the slides were incubated with secondary antibody, followed by colorimetric detection using DAB staining kit (Servicebio, China Cat# G1211). Negative controls were prepared by replacing the primary antibodies with phosphate-buffered saline (PBS). The intensity of immunohistochemistry staining was determined based on five random microscopic fields. Numeric scores were assigned on the percentage of cells stained: 0 (< 5%), 1 (5%-25%), 2 (26%-50%), and 3 (51-75%), and 4 (76-100%). Numeric values were also assigned to express immunohistochemistry staining intensity: 0 (colorless), 1 (light yellow), 2 (brownish yellow), and 3 (brown). Expression was determined by the multiplication of both scores per slide with a final score of 0 representing negative expression (-), while scores 1-4, 5-8, and 9-12 represented weak positivity (+), positive (++), and strong positivity (+++), respectively.

Transfection and induction of DNAJB9 dysfunction via CRISPR/Cas9

To further explore the function of DNAJB9 in choriocarcinoma cell lines DNAJB9 site-specific genetic alterations were carried out as follows: JEG-3 cells were transfected with lentivirus expressing either one of two single guide RNA (sgRNA), DNAJB9-sgRNA1-GFP or DNAJB9-sgRNA2-GFP, each targeting a single nucleotide of the second exon of the DNAJB9 gene, and co-expressing nCas9. The sgRNA sequences are as follows: sgRNA1: 5'-TATCTTAGGTGTGCCAAAAT-3'; sgRNA2: 5'-TGTGAAAGGCCTTCTTGATT-3'.

JEG-3 cells transfected with empty lentivirus were used as negative control. Lentiviruses were obtained from ViGene Biosciences (Shandong, China).

T7 endonuclease 1 enzyme assay

In order to perform PCR proliferation, cells were collected following transfection, and total DNA was extracted from cells using the E.Z.N.A

Genetic similarities however with vast differences

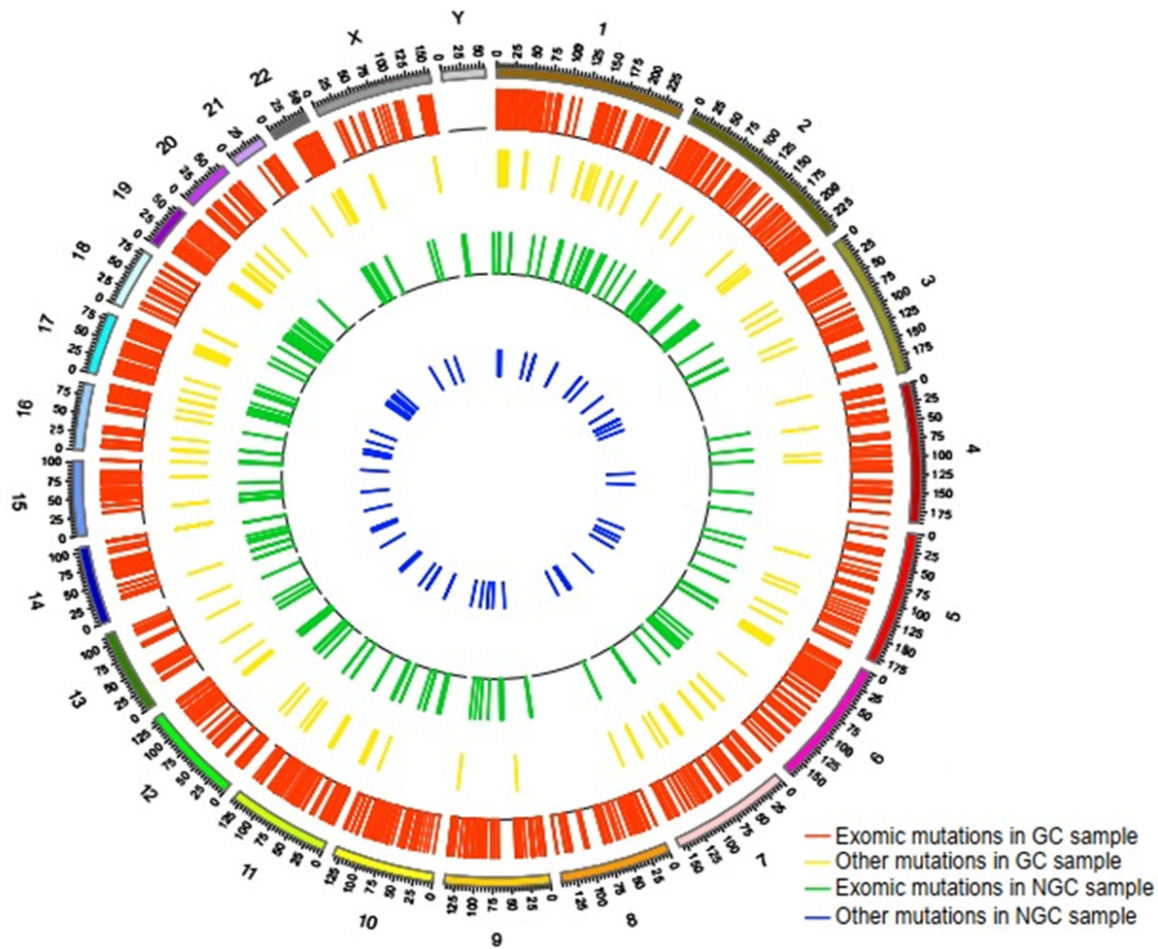


Figure 1. Circos plots summarizing all significant genomic events in GC tumor sample (outer plot) and NGC tumor sample (inner plot).

Tissue DNA Kit (Omega Bio-tek, USA Cat# D3396-01) according to the vendor's protocol. PCR products were then purified using E.Z.N.A Cycle-Pure Kit (Omega Bio-tek, USA Cat# D6492-02) based on instructions provided by the manufacturer. The DNAJB9 primer sequence is as follows: Forward: 5'-TCTCCTCTGTGTATGGCCAGA-3'; Reverse: 5'-TGCTCAGCAGGTGCAATTTG-3'.

Targeting efficiencies were measured using the T7 Endonuclease I (T7E1) Kit (New England BioLabs, USA Cat# M0302S) following the manufacturer's instructions. Detection was performed using agarose gel electrophoresis.

Reverse transcription quantitative real-time PCR for the detection of DNAJB9

Total RNA was extracted from the cells using TRIzol Reagent (Invitrogen, USA Cat# 155960-26) and reverse transcribed into cDNA using

M-MLV reverse transcriptase (Takara, Japan). Reverse transcription quantitative real-time PCR (RT-qPCR) was performed using a Bio-Rad CFX96 system with SYBR Green. The DNAJB9 primer sequence is as follows: Forward: 5'-ATCTTAGGTGTGCCAAAATCG-3'; Reverse: 5'-GACCAAAAAGCCAAAGTCTTT-3'.

The reactions were amplified as follows: 95°C for 3 mins and 40 cycles of 95°C for 10 s, 60°C for 30 s, and 95°C for 15 s.

Western blot analysis

Total cell lysates were prepared in radioimmunoprecipitation assay (RIPA) lysis buffer (Beyotime, China) supplemented with a protease inhibitor cocktail (Roche, Germany). Protein concentrations were determined using Coomassie blue staining. Total lysates (40 µg per sample) were subjected to sodium dodecyl sulfate-polyacrylamide gel electrophoresis (SDS-PAGE)

Genetic similarities however with vast differences

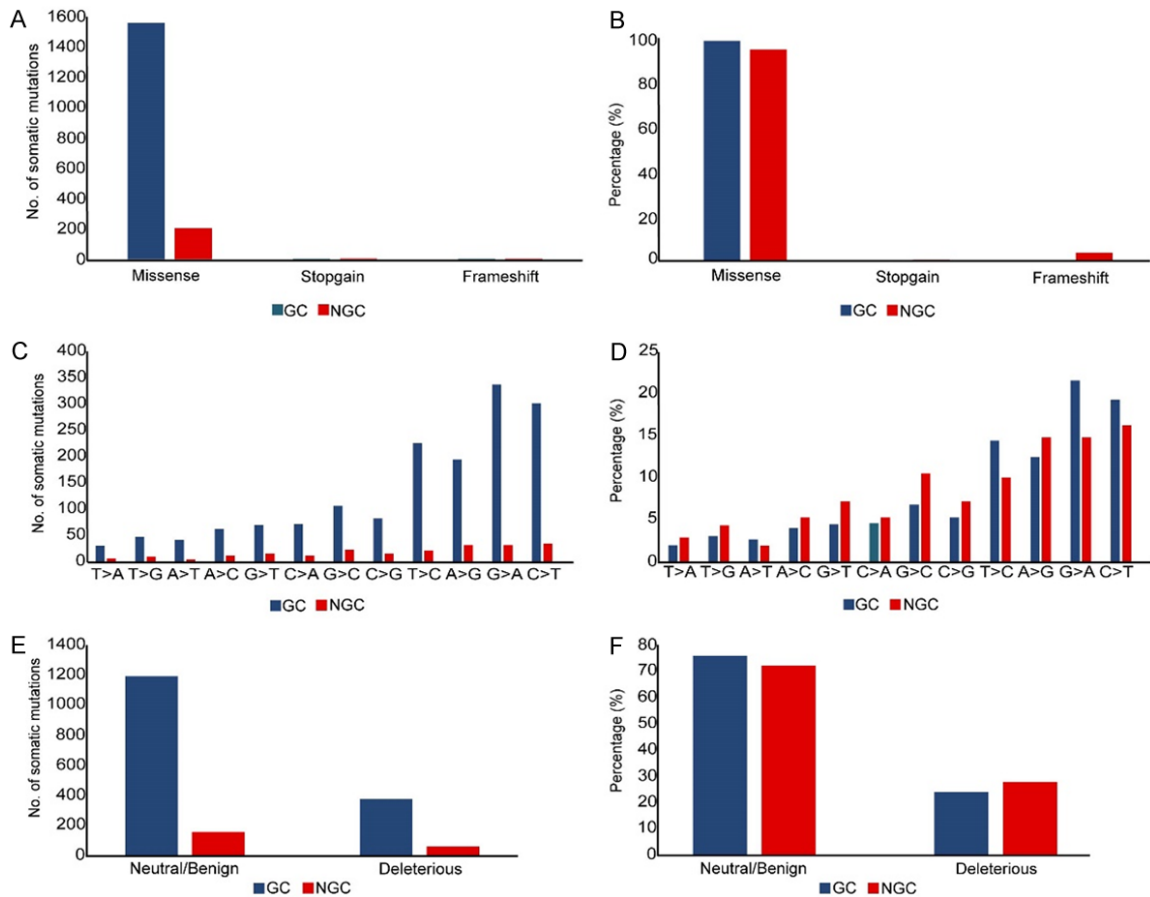


Figure 2. A. Bar chart representation of the number of somatic mutations identified in each choriocarcinoma sample. B. Bar chart representation of the percentage of somatic mutations identified in each choriocarcinoma sample. C. Bar chart representation of the number of different substitutions in missense and stop gain mutations in each choriocarcinoma sample. D. Bar chart representation of the percentage of various substitutions in missense and stop-gain mutations in each choriocarcinoma sample. E. Bar chart representation of the number of the functional impact of mutated genes based on protein predicted scores in each choriocarcinoma sample. F. Bar chart representation of the percentage of the functional impact of mutated genes based on protein predicted scores in each choriocarcinoma sample.

followed by immunoblotting with primary antibodies against the following proteins: *DNAJB9* (1:500, GeneTex, USA Cat# GTX26053), glyceraldehyde 3-phosphate dehydrogenase (GAPDH) (1:4,000, Proteintech Group, China Cat# 60-004-1-Ig), and *TP53* (1:500, ABclonal, USA Cat# A5761). After the membranes were washed, they were incubated with the corresponding horseradish peroxidase-conjugated secondary antibodies (antGENE, China), and the proteins were detected using an enhanced chemiluminescence system (Thermo Fisher Scientific, USA).

Statistics

The data are presented as the mean value \pm standard error of mean (SEM) acquired from at

least three independent experiments. Prism 6.0 GraphPad Software was used to perform statistical analyses. Single comparisons between two groups were done by Student's t-test. Comparison of the ratio of various mutations between GC and NGC was done by Chi-square test. *P* values of ≤ 0.05 were considered statistically significant.

Results

Summary of somatic mutations

Summaries of variants identified in both tumor samples are shown in **Figure 1**. Overall, 1574 and 219 somatic nonsynonymous variants in exons were observed in the GC and NGC tumor samples, respectively. Among the somatic non-

Genetic similarities however with vast differences

synonymous variants in the GC tumor, 1556 (98.86%) missense mutations, 9 (0.57%) stop-gain mutations, and 9 (0.57%) frameshift mutations were observed, while 208 (94.97%) missense mutations, 2 (0.93%) stop-gain mutations, and 9 (4.10%) frameshift mutations were observed in the NGC tumor ($\chi^2 = 24.63$, $P < 0.00001$) (**Figure 2A** and **2B**). The overall rate of transition substitution was 67.54% (1057/1565) and 55.71% (117/210) in the GC and NGC samples, respectively, while the rate of transversion substitution was 32.46% (508/1565) and 44.29% (93/210) in the GC and NGC samples, respectively ($\chi^2 = 11.56$, $P < 0.000673$). Although the transition and transversion substitution counts displayed astonishing differences between the GC and NGC tumors, smaller discrepancies were observed in the actual rates of these two substitution types (**Figure 2C** and **2D**). For instance, 194 and 31 A > G transition substitutions were observed in the GC and NGC samples, respectively. However, this substitution accounted for 12.40% (194/1565) and 14.76% (31/208) in the GC and NGC samples, respectively. 71 and 11 C > A transversion substitutions were highlighted in the GC and NGC samples, respectively. As per the above trend, this substitution accounted for 4.54% (71/1565) and 5.24% (11/210) in the GC and NGC samples, respectively. A similar trend was observed with further analysis using the algorithms/databases as mentioned earlier for variant prediction (**Figure 2E** and **2F**). Though the number of variants predicted to be either benign/neutral or deleterious in the GC sample far exceeded those in the NGC sample, the percentage of either prediction in both samples was staggeringly similar. Benign/neutral variants accounted for 75.98% (1196/1574) and 72.15% (158/219) in the GC and NGC samples, respectively, in contrast to 24.02% (378/1574) and 27.85% (61/219) of variants being deleterious in the GC and NGC samples, respectively ($\chi^2 = 1.53$, $P = 0.22$). All frameshift mutations were classified as pathogenic.

Multiple gene family mutations were observed in both tumors. Of these, 75 zinc finger (*ZNF*), 35 solute carrier (*SLC*), and seven mucin (*MUC*) genes were mutated in the GC tumor. Of the multiple gene family mutations in the NGC tumor, most noteworthy were 18 *MUC* and 4 *ZNF* genes. Twenty-seven somatic mutations

(26 missense mutations, one frameshift mutation) were shared between these two tumors (**Table 2**). Among the somatic nonsynonymous variants of the NGC tumor, two were missense mutations of the second exon of the *DNAJB9* gene (c.T137A:p.F46Y, c.A140G:p.H47R) (**Figure 3A**).

Mutational signatures and KEGG pathway analysis

Mutational analysis revealed two signatures between GC and NGC, which were characterized by C > T mutations (**Figure 3B**). Signature 1 related to the spontaneous deamination of 5-methylcytosine, while signature 5 was of unknown etiology. However, due to limited sample size, further characterization in additional cases is required.

All somatic mutations observed in the GC (15-74) and NGC (219) were subjected to enrichment analysis with the KEGG pathways. We further found that genes in the GC sample were enriched in the following: olfactory transduction, ECM-receptor interaction, protein digestion and absorption, and amoebiasis, while genes in the NGC sample were enriched in the following: olfactory transduction, phagosome, graft-versus-host disease, antigen processing and presentation, and allograft rejection (**Figure 4A-D**; **Table 3**). Additionally, the most significant pathway was olfactory transduction in both GC and NGC samples.

DNAJB9 and p53 expression in GC and NGC samples

DNAJB9, observed to be mutated in the NGC tumor, is a known negative feedback regulator of the tumor suppressor gene *p53*, a tumor suppressor gene which is interestingly known to display upregulated expression in choriocarcinoma [1, 26]. Hence, in light of the relationship between *DNAJB9* and *p53*, we investigated the effects of *DNAJB9* mutations on *p53* expression in choriocarcinoma. **Figure 5A** represents the immunohistochemistry staining for *DNAJB9* and *p53* in the GC and NGC tumor samples. *DNAJB9* was observed to be mainly expressed in the cell membrane and cytoplasm. Based on the scoring method used, *DNAJB9* expression levels in the GC sample displayed strong positivity (+++), while weak positivity (+) was observed in the NGC sample.

Genetic similarities however with vast differences

Table 2. Shared mutations between gestational choriocarcinoma and non-gestational choriocarcinoma samples

Chr	Position	Reference Allele	Tumor Allele	Zygosity	dbSNP ID	Region	Type	Gene	Transcript Name	Exon	CDS Position	Protein Change
14	73575485	A	G	Hetero	rs7494	Exonic	Nonsyn	ACOT2	NM_006821	3	c.A1424G	p.H475R
2	240682792	T	C	Hetero	rs4081908	Exonic	Nonsyn	AQP12B	NM_001102467	1	c.A46	p.T16A
12	107319734	G	C	Hetero	rs961498	Exonic	Nonsyn	BTBD11	NM_001018072	1	c.G794C	p.G265A
12	107319919	G	A	Hetero	rs111260184	Exonic	Nonsyn	BTBD11	NM_001018072	1	c.G979A	p.A327T
1	247111597	A	G	Hetero	rs73135916	Exonic	Nonsyn	C1orf229	NM_207401	1	c.T628C	p.S210P
5	13931231	C	T	Hetero	rs1530496	Exonic	Nonsyn	DNAH5	NM_001369	2	c.G71A	p.G24E
3	75665689	A	G	Hetero	rs200756071	Exonic	Nonsyn	FRG2C	NM_001124759	4	c.A497G	p.E166G
15	72662719	G	A	Hetero	rs200016190	Exonic	Nonsyn	GOLGA6B	NM_018652	11	c.G1315A	p.D439N
15	34386710	C	G	Hetero	rs147828722	Exonic	Nonsyn	GOLGA8A	NM_181077	3	c.G200C	p.R67P
6	31356423	G	C	Hetero	rs1140412	Exonic	Nonsyn	HLA-B	NM_005514	3	c.C363G	c.C363G
17	21415757	G	A	Hetero	rs76265595	Exonic	Nonsyn	KCNJ12	NM_021012	3	c.G415A	p.E139K
17	20467454	G	C	Hetero	rs4985834	Exonic	Nonsyn	LGALS9B	NM_001042685	1	c.C17G	p.S6C
14	39246997	A	G	Hetero	rs11845046	Exonic	Nonsyn	MIA2	NM_054024	4	c.A423G	p.I141M
7	100993727	C	A	Hetero	rs202180008	Exonic	Nonsyn	MUC12	NM_001164462	2	c.C3164A	p.A1055E
9	94325541	G	C	Hetero	rs202099818	Exonic	Nonsyn	NUTM2F	NM_017561	2	c.C410G	p.S137C
2	130074612	G	A	Hetero	rs62165870	Exonic	Nonsyn	POTEF	NM_001099771	17	c.C2860T	p.R954W
2	240042210	A	G	Hetero	rs200217866	Exonic	Nonsyn	PRR21	NM_001080835	1	c.T773C	p.M258T
2	240042322	A	G	Hetero	-	Exonic	Nonsyn	PRR21	NM_001080835	1	c.T661C	p.C221R
9	2828765	C	G	Hetero	rs2173904	Exonic	Nonsyn	PUM3	NM_014878	9	c.G866C	p.R289P
12	100338529	C	G	Hetero	rs56391464	Exonic	Nonsyn	SCYL2	NM_017988	18	c.C2147G	p.T716S
19	460668	C	G	Hetero	rs189741717	Exonic	Nonsyn	SHC2	NM_012435	1	c.G329C	p.G110A
5	94651827	C	A	Hetero	rs6891545	Exonic	Nonsyn	SLF1	NM_032290	7	c.C864A	p.S288R
6	167180694	A	C	Hetero	rs1537172	Exonic	Nonsyn	TCP10L2	NM_001145121	7	c.A831C	p.E277D
13	23593366	T	A	Hetero	rs9550987	Exonic	Nonsyn	TNFRSF19	NM_001204458	3	c.T91A	p.S31T
2	178658787	T	A	Hetero	rs200021871	Exonic	Nonsyn	TTN	NM_001267550	183	c.A37461T	p.E12487D
17	15540420	A	G	Hetero	rs200768112	Exonic	Nonsyn	TVP23C	NM_001135036	6	c.T604C	p.W202R
7	151086813	-	G	Hetero	rs539642617	Exonic	Fshift	AGAP3	NM_001042535	1	c.73dupG	p.G24fs

Abbreviations: Chr: chromosome; Fshift: frameshift; Hetero: heterozygous; Nonsyn: nonsynonymous.

Genetic similarities however with vast differences

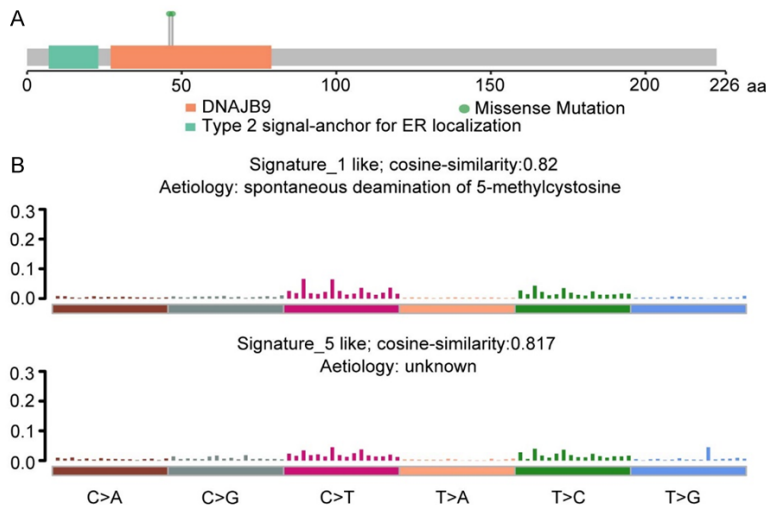


Figure 3. A. Mutation diagram showing the distribution of somatic mutations in the functional domain of DNAJB9. B. Mutational signatures identified in GC and NGC samples, where the y-axis represents the exposure of 96 trinucleotide motifs to the overall signature. Overall, signatures titles represent the best match against validated COSMIC signatures and cosine similarity value with proposed etiology.

In contrast, p53 was observed to be mainly expressed in the nucleus and partly in the cytoplasm. The GC sample displayed weak positivity (+) for p53, while the NGC sample displayed strong positive (+++) p53 expression.

DNAJB9 dysfunction upregulates p53 expression in choriocarcinoma

To explore the function of the *DNAJB9* gene in choriocarcinoma, we designed two sgRNAs (*DNAJB9*-sgRNA1-GFP and *DNAJB9*-sgRNA2-GFP) to achieve site-specific mutations in *DNAJB9* in JEG-3 cells. Successful transfection of designed sgRNAs was confirmed with GFP expression observed via a confocal microscope (Figure 5B). The T7E1 Enzyme Assay confirmed site-specific mutations induced by the CRISPR/Cas9 gene-editing system (Figure 5C). RT-qPCR performed to analyze *DNAJB9* mRNA expression levels showed that downregulation followed site-specific mutations induced by CRISPR/Cas9 gene-editing system (Figure 5D). It was observed that *DNAJB9* protein expression levels were also downregulated, while p53 protein expression levels were upregulated following the induction of these site-specific *DNAJB9* mutations (Figure 5E). These findings taken together prove that site-specific *DNAJB9* mutations induced by the CRISPR/Cas9 gene-editing system induced *DNAJB9* gene dysfunction,

thus down-regulating *DNAJB9* expression which subsequently led to the upregulated expression of p53 in JEG-3 cells.

Discussion

In the current study, we report a pilot analysis of genomic alterations in GC and NGC using WES and put forth the first study of this nature. In our analysis, multiple mutations in the *ZNF*, *SLC*, and *MUC* gene families were observed in both tumor samples, with the GC tumor containing a minimum of twice the number of mutations among these gene families compared to the NGC tumor. These gene families play roles in

transcriptional regulation and the coding of transporters and have been linked to several diseases, including cancer [27-29]. None of the above mutations have been previously associated with choriocarcinoma and may warrant further study.

A keen observation of this study was the overwhelming disparity in the overall number of somatic mutations between the GC and NGC samples when analyzed based on the aforementioned categories. However, both the GC and NGC samples displayed similar total percentages in every category. GC may be androgenetic or biparental in its genetic composition [6]. Nevertheless, this case of GC was diagnosed less than one year following an antecedent term pregnancy, a key factor for proceeding with the notion that this case of GC was biparental in its genetic composition. Such a genetic makeup would explain the large number of somatic mutations far exceeding that of NGC. In contrast, NGC is unrelated to any form of gestation and is, therefore, genetically linked to the patient [6]. This may explain fewer somatic mutations observed in our NGC tumor. Notwithstanding the genetic composition of NGC, it could contain karyotypic aberrations [9]. Nonetheless, both samples displayed similar ratios of somatic mutations across all categories analyzed. Hence, we believe that alth-

Genetic similarities however with vast differences

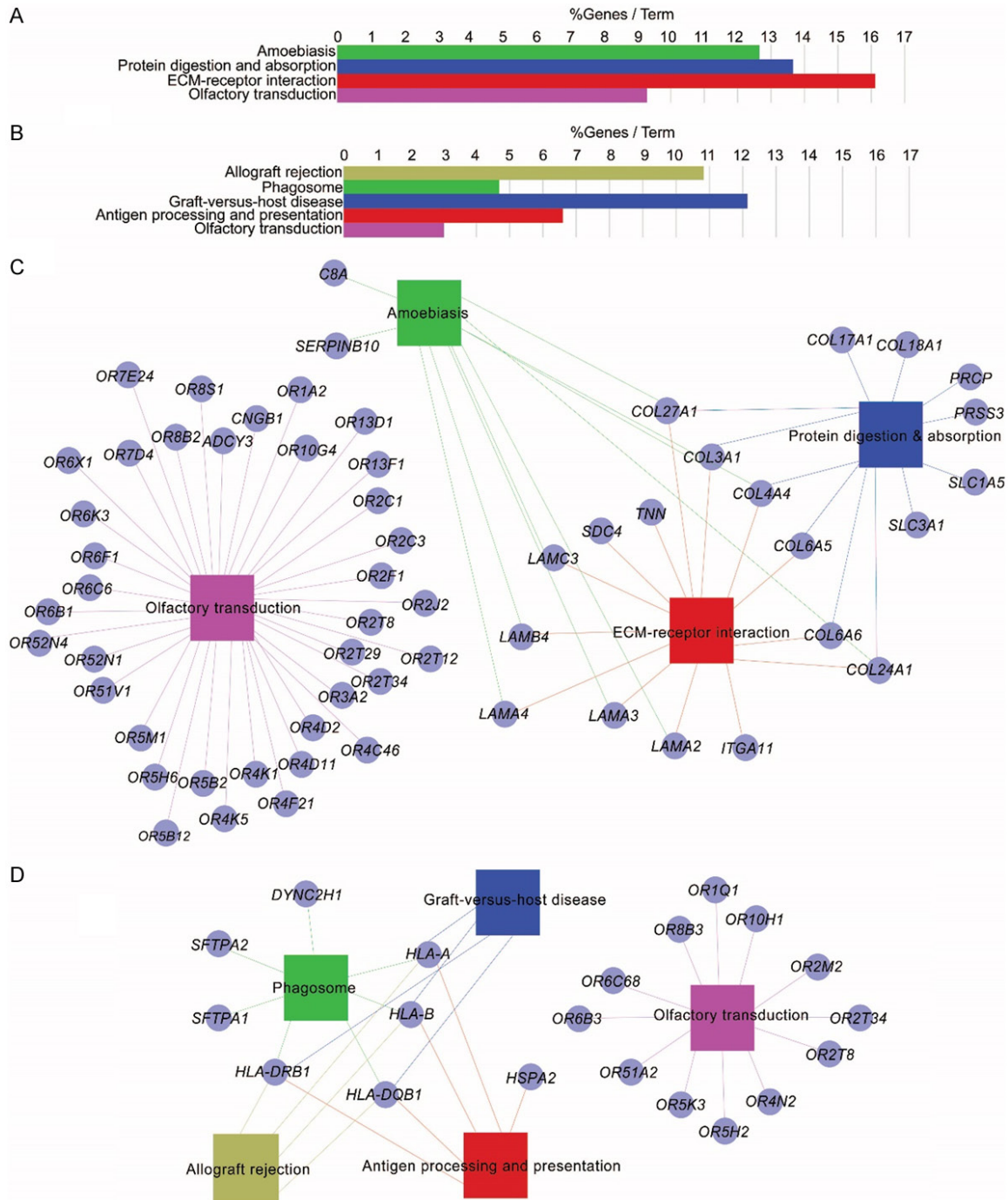


Figure 4. A. Bar chart representation of the enrichment mutated genes observed in the GC tumor in KEGG pathways. B. Bar chart representation of the enrichment mutated genes observed in the NGC tumor in KEGG pathways. C. Cytoscape representation of mutated genes found in the GC sample in KEGG pathways. D. Cytoscape representation of mutated genes observed in the NGC sample in KEGG pathways.

ough the origin of choriocarcinoma plays a fundamental role in its genetic composition, both subtypes may be similar in regards to the ratio of different genetic events, possibly meaning that the number and type of genetic events

may not have a direct influence on this disease. Specific genetic anomalies occurring in key genes may be a more significant factor in determining the phenotypic characteristics of GC and NGC.

Genetic similarities however with vast differences

Table 3. KEGG pathway analysis of somatic mutations in GC and NGC samples

Pathway ID	GO Term	P-value	Associated Genes (%)	N. of Genes	Associated Genes
GC					
hsa04740	Olfactory transduction	5.0E-4	9.27	37	<i>ADCY3, CNGB1, OR1A2, OR10G4, OR13D1, OR13F1, OR2C1, OR2C3, OR2F1, OR2J2, OR2T12, OR2T29, OR2T34, OR2T8, OR3A2, OR4C46, OR4D2, OR4D11, OR4F21, OR4K1, OR4K5, OR5B12, OR5H6, OR5M1, OR51V1, OR52N1, OR52N4, OR6B1, OR6C6, OR6F1, OR6K3, OR6X1, OR7D4, OR7E24, OR8B2, OR8S1</i>
hsa04512	ECM-receptor interaction	4.1E-4	16.10	14	<i>COL3A1, COL4A4, COL6A5, COL6A6, COL24A1, COL27A1, ITGA11, LAMA2, LAMA3, LAMA4, LAMB4, LAMC3, SDC4, TNN</i>
hsa04974	Protein digestion and absorption	4.8E-3	13.64	12	<i>COL3A1, COL4A4, COL6A5, COL6A6, COL17A1, COL18A1, COL24A1, COL27A1, PRCP, PRSS3, SLC1A5, SLC3A1</i>
hsa05146	Amoebiasis	4.3E-2	12.64	11	<i>COL3A1, COL4A4, COL17A1, COL18A1, C8A, LAMA2, LAMA3, LAMA4, LAMB4, LAMC3, SERPINB10</i>
NGC					
hsa04740	Olfactory transduction	8.6E-5	3.01	12	<i>OR1Q1, OR10H1, OR2M2, OR2T34, OR2T8, OR4N2, OR5H2, OR5K3, OR51A2, OR6B3, OR6C68, OR8B3</i>
hsa04145	Phagosome	6.3E-4	4.67	7	<i>DYNC2H1, HLA-A, HLA-B, HLA-DQB1, HLA-DRB1, SFTPA1, SFTPA2</i>
hsa05332	Graft-versus-host disease	1.6E-3	12.12	4	<i>HLA-A, HLA-B, HLA-DQB1, HLA-DRB1</i>
hsa04612	Antigen processing and presentation	2.0E-3	6.58	5	<i>HSPA2, HLA-A, HLA-B, HLA-DQB1, HLA-DRB1</i>
hsa05330	Allograft rejection	2.2E-3	10.81	4	<i>HLA-A, HLA-B, HLA-DQB1, HLA-DRB1</i>

Abbreviation: GO Term: gene ontology term.

Genetic similarities however with vast differences

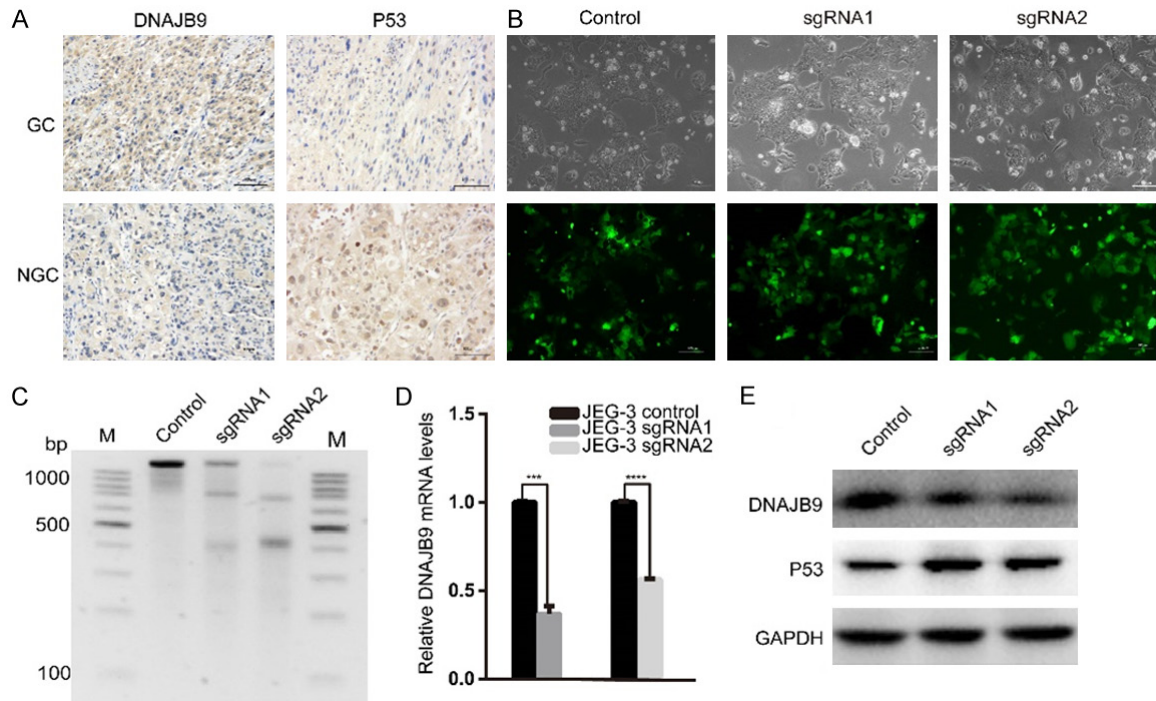


Figure 5. (A) Immunohistochemistry staining ($\times 200$) for *DNAJB9* and *p53*. (B) Expression of *DNAJB9*-sgRNA1-GFP and *DNAJB9*-sgRNA2-GFP in JEG-3 cell detected using an inverted fluorescence microscope ($\times 200$). (C) The detection of targeted deletion mutation of *DNAJB9* in which sgRNA1 produced 300-bp and 580-bp products, and sgRNA2 produced 340-bp and 540-bp products. (D) *DNAJB9* mRNA levels were assessed in Cas9 + *DNAJB9*-sgRNA1, Cas9 + *DNAJB9*-sgRNA2, and empty lentivirus (control) JEG-3 cells using RT-qPCR. (E) Western blotting analysis confirmed *DNAJB9* downregulation and *p53* overexpression in JEG-3 cells transfected with Cas9 + *DNAJB9*-sgRNA1 and Cas9 + *DNAJB9*-sgRNA2 compared to control. Every bar represents the mean \pm SEM of three independent experiments in (D). *** $P < 0.001$ by Student's t-test.

Our results also showed that the GC sample contained mutated genes which were most enriched in ECM-receptor interaction. Previous reports have highlighted that complex ECM interactions play pivotal roles in the regulation of homeostasis, inflammation, morphogenesis, proliferation, differentiation, and migration [30, 31]. Any dysregulation of these interactions induces a host of pathological conditions, including invasive cancer [32]. Here, the dysfunction of ECM interactions further stimulates cancer progression via cancer cell polarity, signaling, and increased motility [33]. Moreover, both the GC and NGC samples contained mutated genes which were highlighted to be enriched in olfactory transduction. Olfactory receptors (ORs) are members of G-protein coupled receptors, the largest gene family in the human genome [34, 35]. Previously, ORs were thought to only function in the olfactory epithelium and were ignored in regards to tumorigenesis. Recent studies have since refuted this notion and proven that ORs are linked to several cancers

and influence many levels of carcinogenesis, including proliferation, migration, invasion, etc. [34, 36-38].

Interestingly, the NGC tumor contained mutated genes most enriched in graft-versus-host disease and highly enriched in allograft rejection. Previous reports have highlighted GC as a tissue allograft, in contrast to NGC, which originated from the patient [6]. Thus, findings of genetic mutations associated with these pathways in the NGC tumor are rather peculiar. Therefore, we propose that dysfunction of these pathways may be responsible for the phenotypic characteristics of choriocarcinoma, namely its highly metastatic nature, and that the identification of these pathways should prompt further investigation of these pathways for targeted treatment of choriocarcinoma. Additionally, the roles of graft-versus-host disease and allograft rejection pathways in choriocarcinoma, especially NGC, should be further evaluated.

Genetic similarities however with vast differences

A well-known correlation has been drawn between the mutations of the tumor suppressor gene *p53* and many cancers. Intriguingly, no *p53* mutations were observed in either choriocarcinoma sample. However, several studies have highlighted *p53* expression to be upregulated in choriocarcinoma [1, 39]. Many studies have explored *p53* regulation and have highlighted several genes which inhibit *p53* function by acting as negative feedback regulators [40-42]. Among these is *DNAJB9*, a gene which regulates ATPase activity of Hsp70s [43-45]. According to Lee et al., *p53* induces *DNAJB9* expression, which then acts as a negative feedback regulator of *p53* via the Ras/Raf/ERK pathway and nuclear interaction [26]. Astonishingly, we found two mutations of the *DNAJB9* gene in the NGC sample, the only of these *p53* regulator genes mutated in either choriocarcinoma sample. Therefore, in order to further investigate the relationship between *DNAJB9* mutation and *p53* overexpression in choriocarcinoma, we induced site-specific *DNAJB9* mutations and demonstrated the effect of these mutations on *p53* expression in JEG-3 cells. Compared with the control group, *DNAJB9* mRNA and protein expression levels in JEG-3 cells were downregulated in both Cas9 + *DNAJB9*-sgRNA transfected groups. We further confirmed that compared to the control group, *p53* protein expression levels in JEG-3 cells were upregulated in both Cas9 + *DNAJB9*-sgRNA transfected groups. These findings demonstrated that site-specific *DNAJB9* mutations induced by CRISPR/Cas9 triggered *DNAJB9* gene dysfunction, thus interrupting its negative feedback regulation of *p53*, finally leading to *p53* overexpression, hence a probable cause of *p53* upregulation in choriocarcinoma. This also further highlights the relationship between *DNAJB9* and *p53*.

However, this study is not without limitations. First, this study contains a small sample size. We do believe that in light of this limitation and our exciting discoveries, there is a need for further investigation involving a larger sample size in which these two types of choriocarcinoma are further genetically analyzed. Moreover, we were unable to gain access to paternal DNA in order to eliminate paternal germline mutations in the GC case. We propose that further investigations include the elimination of paternal germline mutations in order to only identify and analyze somatic mutations.

In conclusion, this study represents a pilot effort which used NGS to gain a much better understanding of the molecular biology of the choriocarcinoma as both GC and NGC are molecularly distinct, and will undoubtedly provide much guidance as we embark on larger related projects. We identified several somatically mutated genes in either type of choriocarcinoma with specific mutations being presented as possible factors in the clinical characteristics of choriocarcinoma. Additionally, via the use of CRISPR/Cas9, we further underscored the relationship between *DNAJB9* and *p53* and presented *DNAJB9* mutations as a possible causative factor in *p53* upregulation in the JEG-3 choriocarcinoma cell line.

Acknowledgements

This work was supported by the National Science Foundation of China (grant numbers 81630060; 81772775); the National Key Research and Development Program of China (grant number 2016YFC0902901) and the National 973 Project of China (grant number 2015CB553903).

Disclosure of conflict of interest

None.

Address correspondence to: Dr. Peng Wu, Department of Gynecologic Oncology, Tongji Hospital, Tongji Medical College, Huazhong University of Science and Technology, Wuhan 430030, Hubei Province, China. Tel: +86-13995573729; E-mail: pengwu8626@tjh.tjmu.edu.cn

References

- [1] Cheung AN, Zhang HJ, Xue WC and Siu MK. Pathogenesis of choriocarcinoma: clinical, genetic and stem cell perspectives. *Futur Oncol* 2009; 5: 217-231.
- [2] Shih IM. Gestational trophoblastic neoplasia-pathogenesis and potential therapeutic targets. *Lancet Oncol* 2007; 8: 642-650.
- [3] Dilek S, Pata Ö, Tok E and Polat A. Extraovarian non-gestational choriocarcinoma in a postmenopausal woman. *Int J Gynecol Cancer* 2004; 14: 1033-1035.
- [4] Fisher RA, Savage PM, MacDermott C, Hook J, Sebire NJ, Lindsay I and Seckl MJ. The impact of molecular genetic diagnosis on the management of women with hCG-producing malignancies. *Gynecol Oncol* 2007; 107: 413-419.

Genetic similarities however with vast differences

- [5] O'Neill CJ, Houghton F, Clarke J and McCluggage WG. Uterine gestational choriocarcinoma developing after a long latent period in a postmenopausal woman: the value of DNA polymorphism studies. *Int J Surg Pathol* 2008; 16: 226-229.
- [6] Savage J, Adams E, Veras E, Murphy KM and Ronnett BM. Choriocarcinoma in women: analysis of a case series with genotyping. *Am J Surg Pathol* 2017; 41: 1593-1606.
- [7] Hirata Y, Yanaihara N, Yanagida S, Fukui K, Iwadate K, Kiyokawa T and Tanaka T. Molecular genetic analysis of non-gestational choriocarcinoma in a postmenopausal woman: a case report and literature review. *Int J Gynecol Pathol* 2012; 31: 364-368.
- [8] Olson MT, Gocke CD, Giuntoli RL and Shih IM. Evolution of a trophoblastic tumor from an endometrioid carcinoma-A morphological and molecular analysis. *Int J Gynecol Pathol* 2011; 30: 117-120.
- [9] Hoffner L and Surti U. The genetics of gestational trophoblastic disease: a rare complication of pregnancy. *Cancer Genet* 2012; 205: 63-77.
- [10] Aranake-Chrisinger J, Huettnner PC, Hagemann AR and Pfeifer JD. Use of short tandem repeat analysis in unusual presentations of trophoblastic tumors and their mimics. *Hum Pathol* 2016; 52: 92-100.
- [11] Guo J, Zhong C, Liu Q, Xu J, Zheng Y, Xu S, Gao Y, Guo Y, Wang Y, Luo Q and Jiang J. Intracranial choriocarcinoma occurrence in males: two cases and a review of the literature. *Oncol Lett* 2013; 6: 1329-1332.
- [12] Desai NR, Gupta S, Said R, Desai P and Dai Q. Choriocarcinoma in a 73-year-old woman: a case report and review of the literature. *J Med Case Rep* 2010; 4: 379.
- [13] Kanehira K, Starostik P, Kasznica J and Khoury T. Primary intraplacental gestational choriocarcinoma: histologic and genetic analyses. *Int J Gynecol Pathol* 2013; 32: 71-75.
- [14] Mello JB, Ramos Cirilo PD, Michelin OC, Custódio Domingues MA, Cunha Rudge MV, Rogatto SR and Maestá I. Genomic profile in gestational and non-gestational choriocarcinomas. *Placenta* 2017; 50: 8-15.
- [15] Wang Y, Yang Y, Teng F, Zhang H and Xue F. Pure non-gestational uterine choriocarcinoma in a postmenopausal Chinese woman confirmed with short tandem repeat analysis. *Am J Obstet Gynecol* 2014; 211: e1-3.
- [16] Yamamoto E, Niimi K, Shinjo K, Yamamoto T, Fukunaga M and Kikkawa F. Identification of causative pregnancy of gestational trophoblastic neoplasia diagnosed during pregnancy by short tandem repeat analysis. *Gynecol Oncol Reports* 2014; 9: 3-6.
- [17] Wang K, Li M and Hakonarson H. ANNOVAR: functional annotation of genetic variants from high-throughput sequencing data. *Nucleic Acids Res* 2010; 38: e164.
- [18] Richards S, Aziz N, Bale S, Bick D, Das S, Gastier-Foster J, Grody WW, Hegde M, Lyon E, Spector E, Voelkerding K and Rehm HL; ACMG Laboratory Quality Assurance Committee. Standards and guidelines for the interpretation of sequence variants: a joint consensus recommendation of the American college of medical genetics and genomics and the association for molecular pathology. *Genet Med* 2015; 17: 405-424.
- [19] Krzywinski M, Schein J, Birol I, Connors J, Gascoyne R, Horsman D, Jones SJ and Marra MA. Circos: an information aesthetic for comparative genomics. *Genome Res* 2009; 19: 1639-1645.
- [20] Mayakonda A, Lin DC, Assenov Y, Plass C and Koeffler HP. Maftools: efficient and comprehensive analysis of somatic variants in cancer. *Genome Res* 2018; 28: 1747-1756.
- [21] Dennis G Jr, Sherman BT, Hosack DA, Yang J, Gao W, Lane HC and Lempicki RA. DAVID: database for annotation, visualization, and integrated discovery. *Genome Biol* 2003; 4: P3.
- [22] Huang DW, Sherman BT, Tan Q, Kir J, Liu D, Bryant D, Guo Y, Stephens R, Baseler MW, Lane HC and Lempicki RA. DAVID bioinformatics resources: expanded annotation database and novel algorithms to better extract biology from large gene lists. *Nucleic Acids Res* 2007; 35: W169-75.
- [23] Kanehisa M, Sato Y, Kawashima M, Furumichi M and Tanabe M. KEGG as a reference resource for gene and protein annotation. *Nucleic Acids Res* 2016; 44: D457-D462.
- [24] Kanehisa M, Furumichi M, Tanabe M, Sato Y and Morishima K. KEGG: new perspectives on genomes, pathways, diseases and drugs. *Nucleic Acids Res* 2017; 45: D353-D361.
- [25] Shannon P, Markiel A, Ozier O, Baliga NS, Wang JT, Ramage D, Amin N, Schwikowski B and Ideker T. Cytoscape: a software environment for integrated models of biomolecular interaction networks. *Genome Res* 2003; 13: 2498-504.
- [26] Lee HJ, Kim JM, Kim KH, Heo JI, Kwak SJ and Han JA. Genotoxic stress/p53-induced DNAJB9 inhibits the pro-apoptotic function of p53. *Cell Death Differ* 2015; 22: 86-95.
- [27] Stransky N, Egloff AM, Tward AD, Kostic AD, Cibulskis K, Sivachenko A, Kryukov GV, Lawrence MS, Sougnez C, McKenna A, Shefler E, Ramos AH, Stojanov P, Carter SL, Voet D, Cortés ML, Auclair D, Berger MF, Saksena G, Guiducci C, Onofrio RC, Parkin M, Romkes M, Weissfeld JL, Seethala RR, Wang L, Rangel-Es-

Genetic similarities however with vast differences

- careño C, Fernandez-Lopez JC, Hidalgo-Miranda A, Melendez-Zajgla J, Winckler W, Ardlie K, Gabriel SB, Meyerson M, Lander ES, Getz G, Golub TR, Garraway LA and Grandis JR. The mutational landscape of head and neck squamous cell carcinoma. *Science* 2011; 333: 1157-1160.
- [28] Perland E and Fredriksson R. Classification systems of secondary active transporters. *Trends Pharmacol Sci* 2017; 38: 305-315.
- [29] Kufe DW. Mucins in cancer: function, prognosis and therapy. *Nat Rev Cancer* 2009; 9: 874-885.
- [30] Naba A, Clauser KR, Hoersch S, Liu H, Carr SA and Hynes RO. The matrisome: in silico definition and in vivo characterization by proteomics of normal and tumor extracellular matrices. *Mol Cell Proteomics* 2012; 11: M111.014647.
- [31] Hynes RO. The extracellular matrix: not just pretty fibrils. *Science* 2009; 326: 1216-1219.
- [32] Bonnans C, Chou J and Werb Z. Remodelling the extracellular matrix in development and disease. *Nat Rev Mol Cell Biol* 2014; 15: 786-801.
- [33] Gilkes DM, Semenza GL and Wirtz D. Hypoxia and the extracellular matrix: drivers of tumour metastasis. *Nat Rev Cancer* 2014; 14: 430-439.
- [34] Weber L, Al-Refae K, Ebbert J, Jägers P, Altmüller J, Becker C, Hahn S, Gisselmann G and Hatt H. Activation of odorant receptor in colorectal cancer cells leads to inhibition of cell proliferation and apoptosis. *PLoS One* 2017; 12: e0172491.
- [35] Zhong H and Neubig RR. Regulator of G protein signaling proteins: novel multifunctional drug targets. *J Pharmacol Exp Ther* 2001; 297: 837-845.
- [36] Sanz G, Leray I, Dewaele A, Sobilo J, Lerondel S, Bouet S, Grebert D, Monnerie R, Pajot-Augy E and Mir LM. Promotion of cancer cell invasiveness and metastasis emergence caused by olfactory receptor stimulation. *PLoS One* 2014; 9: e85110.
- [37] Massberg D, Simon A, Haussinger D, Keitel V, Gisselmann G, Conrad H and Hatt H. Monoterpene (-)-citronellal affects hepatocarcinoma cell signaling via an olfactory receptor. *Arch Biochem Biophys* 2015; 566: 100-109.
- [38] Zhang X, Bedigian AV, Wang W and Eggert US. G protein-coupled receptors participate in cytoskeleton. *Cytoskeleton (Hoboken)* 2012; 69: 810-818.
- [39] Fulop V, Mok SC, Genest DR, Gati I, Doszpod J and Berkowitz RS. p53, p21, Rb and mdm2 oncoproteins. Expression in normal placenta, partial and complete mole, and choriocarcinoma. *J Reprod Med* 1998; 43: 119-127.
- [40] Han JA, Kim JI, Ongusaha PP, Hwang DH, Ballou LR, Mahale A, Aaronson SA and Lee SW. p53-mediated induction of Cox-2 counteracts p53- or genotoxic stress-induced apoptosis. *EMBO J* 2002; 21: 5635-5644.
- [41] Ongusaha PP, Kim JI, Fang L, Wong TW, Yancopoulos GD, Aaronson SA and Lee SW. p53 induction and activation of DDR1 kinase counteract p53-mediated apoptosis and influence p53 regulation through a positive feedback loop. *EMBO J* 2003; 22: 1289-1301.
- [42] Leng RP, Lin Y, Ma W, Wu H, Lemmers B, Chung S, Parant JM, Lozano G, Hakem R and Benchimol S. Pirh2, a p53-induced ubiquitin-protein ligase, promotes p53 degradation. *Cell* 2003; 112: 779-791.
- [43] Houry W. Chaperone-assisted protein folding in the cell cytoplasm. *Curr Protein Pept Sci* 2001; 2: 227-244.
- [44] Qiu XB, Shao YM, Miao S and Wang L. The diversity of the DnaJ/Hsp40 family, the crucial partners for Hsp70 chaperones. *Cell Mol Life Sci* 2006; 63: 2560-2570.
- [45] Vos MJ, Hageman J, Carra S and Kampinga HH. Structural and functional diversities between members of the human HSPB, HSPH, HSPA, and DNAJ chaperone families. *Biochemistry* 2008; 47: 7001-7011.